Received: 11 November 2023 | Revised: 16 April 2024 | Accepted: 3 May 2024

DOI: 10.1111/ppl.14351

TECHNICAL ADVANCE

Physiologia Plantarum

Protein Detection and Localization in Plant Cells Using Spot-Tagging

Andriani Mentzelopoulou[1,2*] | Chen Liu[3*] | Panagiotis Nikolaou Moschou[1,2,4]

[1]Department of Biology, University of Crete, Heraklion, Greece

[2]Institute of Molecular Biology and Biotechnology, Foundation for Research and Technology – Hellas, Heraklion, Greece

[3]State Key Laboratory of Biocontrol, Guangdong Key Laboratory of Plant Resources, School of Life Sciences, Sun Yat–Sen University, Guangzhou, China

[4]Department of Molecular Sciences, Uppsala BioCenter, Swedish University of Agricultural Sciences and Linnean Center for Plant Biology, Uppsala, Sweden

Correspondence
Chen Liu,
Email: liuch668@mail.sysu.edu.cn

Funding information
Fondation Sante; IMBB-FORTH start-up funding; Hellenic Foundation for Research and Innovation, Grant/Award Numbers: 06526, 1264; HORIZON EUROPE Marie Sklodowska-Curie Actions, Grant/Award Number: 872969

Edited by V.G. Reddy

Abstract

Fluorescent labelling of proteins enables the determination of their spatiotemporal localization but, sometimes, it can perturb their activity, native localization, and functionality. Spot-tag is a12-amino acid peptide recognized by a single–domain nanobody and could potentially resolve the issues associated with large fluorescence tags due to its small size. Here, using as an example the microtubule motor CENTROMERIC PROTEIN E–RELATED KINESIN 7.3 (KIN7.3), we introduce the spot–tag for protein labelling in fixed and living plant cells. Spot–tagging and detection by an anti-spot nanobody of ectopically expressed KIN7.3 did not interfere with its native localization. Most importantly, our spot-tagging pipeline facilitated the localization of KIN7.3 much more rapidly and likely accurately than labelling with large fluorescent proteins or even immunolocalization approaches. We should, though, note some limitations we have not resolved yet. Spot–tagging is functional only in fixed cells; it is available only as two fluorophores and may create a noisy background during imaging. However, we foresee that, besides the limitations of this method, spot-tagging will apply to many proteins, offsetting activity perturbations and low photon quantum yields of other protein-tagging approaches.

1 | INTRODUCTION

Most labelling strategies exploit antibodies or proteins fused to various stable or photoactivatable fluorescent proteins (FPs) or fluorogenic-labelling enzymes, e.g. the Halo-, CLIP-, or SNAP-tag (Virant et al. 2018). Conventional antibodies introduce significant linkage errors (i.e., by displacing the fluorophore from the protein of interest by several nm), while large protein/enzyme tags may affect expression, cellular localization, folding and/or activity. Although small peptidic epitopes (e.g. FLAG-, HA-, or myc-tag) are widely used, they may not provide sufficient labelling, although they can also be arranged in tandem arrays to recruit medium-affine binding antibodies.

Instead of using antibodies, a 15-amino-acid peptide tag can be probed by high-avid fluorescently labelled monomeric streptavidin, which, however, can be affected by the binding of endogenously biotinylated proteins, especially in plant cells (Liu et al. 2023a, Liu et al. 2024). Alternatively, reversibly on–/off–binding labels in point accumulation for imaging of nanoscale topography (PAINT) microscopy allow for a continuous and, therefore, ultra-high-density readout as they are not limited by a predefined fluorophore tagging pattern (Schnitzbauer et al. 2017). Yet, this approach can only be used for membranes or DNA combined with illumination–confined arrangements (e.g., surface–near or light–sheet illuminations).

As a promising substitute for conventional antibodies, small-sized nanobodies (antibody fragments derived from heavy-chain-only camelid antibodies) coupled with organic dyes,

* These authors contributed equally to this work

e.g. ATTO probes, were relatively recently introduced (Virant et al. 2018). Despite their capability to directly probe endogenous antigens, the *de novo* production of nanobodies and their validation is cumbersome and time-consuming; only a very limited number of microscopy–compatible nanobodies are available. Due to their applicability for nanoscopy of widely used FP-fusions, GFP- and RFP-nanobodies became extremely popular tools. This strategy, however, relies on the correct expression of FP–fusions and does not cope with problems arising from mislocalization, steric hindrances or dysfunction. Thus, nanobodies directed against short and functionally inert tags might prove advantageous.

The versatile labelling and detection strategy comprising the short and inert "spot" peptide tag (PDRKAAVSHWQQ; "spot-tag") and a corresponding high-affinity bivalent nanobody (anti-spot nanobody fused to ATTO) has been successfully used in animal cells (Virant et al. 2018). Here, we refine the spot-tagging approach for high-resolution imaging of plant cells. We demonstrate the benefits of this approach in fixed and living cells, using as a proof-of-concept the CENTROMERIC PROTEIN E-RELATED KINESIN-SEPARASE COMPLEX (KISC) KINESIN 7.3 (KIN7.3).

2 | MATERIALS AND METHODS

2.1 | Plant material and growth conditions

Arabidopsis thaliana Col–0 or KIN7.3pro:GFP–KIN7.3/35Spro:MAP4^{MBD} (Moschou et al. 2016) seedlings were grown on vertical plates containing half-strength Murashige and Skoog medium (Duchefa Biochemie; Product Number M0222.0050), supplemented with 1% (w/v) sucrose (Merck; Product Number 1.07651.1000) and 0.8% (w/v) plant agar (Duchefa Biochemie; Product Number P1001.0500). *Nicotiana benthamiana* plants were directly grown on soil. Plant growth was done at 22°C on a 16 h/8 h light/dark cycle and light intensity of 150 µE m^{-2} s^{-1} in a photostable growth chamber and with a fixed relative humidity of 65% (FitoClima 6001.200; Aralab 1200). *Arabidopsis* plants were transformed according to Clough and Bent (1998) using *Agrobacterium tumefaciens* strain GV3101 carrying *RPS5apro:HF–spot–KIN7.3–myc* or *RPS5apro:HF–spot–KIN7.3–tagRFP* construct in a pGWB–based vector (Nakagawa et al. 2007).

2.2 | Molecular Biology and Vectors Construction

KIN7.3 coding sequence was amplified from *Arabidopsis thaliana* first-strand cDNA template via RT–PCR. The PCR product was cloned in pDONR221 and subsequently in pGWB402 Gateway vector by BP and LR Gateway recombination reactions, respectively. Sequences of the primers used in this study are available in Table S1. The spot-tag sequence introduced was CCTGATAGAGTTAGAGCTGTTTCTC ATTGGTCTTCT.

2.3 | Agroinfiltration

Agrobacterium tumefaciens GV3101 strain, carrying *RPS5apro:HF–spot–KIN7.3–myc* or *KIN7.3pro:KIN7.3–spot*, was cultured at 28°C in Yeast Extract Peptone (YEP) liquid medium [1% (w/v) yeast extract, 1% (w/v) peptone, 0.5% (w/v) NaCl] supplemented with 50 µg/mL spectinomycin and 50 µg/mL rifampicin. Bacteria were harvested by centrifugation at 2,800 *g* for 10 min and the pellet was re-suspended in buffer containing 10 mM 4–Morpholineethanesulfonic acid (MES) pH 5.7, 10 mM $MgCl_2$ and 200 µM acetosyringone; the bacteria were left agitating for 2–4 h at 28°C. Agrobacteria were harvested, again, respectively, and infiltrated into leaves of *N. benthamiana* at a final OD_{600} of 0.4, while co-expressed with a p19 silencing suppressor (Johansen & Carrington, 2001). Approximately six-week-old *N. benthamiana* leaves were used for the infiltration and imaging was done 3–4 days post–infiltration.

2.4 | Phenotypic analyses and drug treatments

For quantification of phenotypes, seeds were surface-sterilized by sodium hypochlorite (12% v/v), plated on ½ MS medium and seedlings were grown vertically. Taxol and oryzalin treatments were done in liquid ½ MS at a final concentration of 10 µM for 1 h at RT [stock solutions were prepared at 10 mM in Dimethyl sulfoxide (DMSO)]. The same volume of DMSO was added to the mock seedlings as a control.

2.5 | Spot tag detection

Seedlings from T2 generation of *A. thaliana RPS5apro:HF–spot–KIN7.3–myc* or *RPS5apro:HF–spot–KIN7.3* ("HF" stands for His-FLAG tags) expressing transgenic lines were fixed in fixation buffer for 1 h [3.7% paraformaldehyde (PFA; dissolved in warm ddH_2O supplemented with 2 drops of 0.1 N KOH), 50 mM piperazine–N,N′–bis (2–ethane sulfonic acid) (PIPES), 5 mM ethylene glycol tetraacetic acid (EGTA), 2 mM $MgSO_4$, 0.4% (v/v) Triton X–100]. Roots were separated from the seedlings using a razor blade and washed with phosphate-buffered saline/0.01% (v/v) Tween–20 (PBST) buffer and next, they were treated with driselase enzyme mix for 7 min [2% (w/v) Driselase (Sigma) in 0.4 M Mannitol, 5 mM ethylene glycol tetraacetic acid (EGTA), 15 mM 2–(N–morpholino) ethane sulfonic acid (MES), pH 5.6, 1 mM phenylmethylsulfonyl fluoride protease inhibitor (PMSF; Sigma)].

Epitope blocking was done for 30 min at RT using 3% (w/v) Bovine Serum Albumin (BSA)/PBST. Then, the roots were incubated overnight at 4°C in anti-myc mouse primary antibody (1:250, Roche in blocking solution) or in anti-γ-TUBULIN primary antibody (1:100, Sigma in blocking solution) and washed 3 times in PBST. The roots were incubated overnight at 4°C with the secondary anti-mouse (1:500; Jackson immunoreactive, conjugated to Rhodamine Red or Alexa647) and eba488–10 Spot-Label ATTO488 (1:50–1:2,000,

Chromotek) diluted in PBS supplemented with 2% (w/v) BSA. After washing with PBST buffer supplemented with DAPI (4′,6-diamidino-2-phenylindole), roots were mounted in Vectashield (Vector Laboratories) mounting medium.

N. benthamiana leaves were harvested 3–4 days post-infiltration with the corresponding Agrobacteria carrying the constructs of interest (i.e., HF–spot–KIN7.3–myc or KIN7.3pro:GFP–KIN7.3). Small cuts from the infiltrated regions were incubated for 1 h in anti-Spot-Tag VHH/Nanobodies conjugated to the organic fluorophore ATTO488 (Chromotek), diluted 1:1,000 in 10 mM Tris–HCl solution pH 7.5, adjusted with HCl.

The fluorescent images (micrographs) were acquired at RT using the Leica SP8 inverted confocal microscope, with a 40x objective (N.A. = 1.2), pinhole adjusted to 1 airy unit and mounting medium ddH_2O. The excitation wavelength was 488 nm (emission 506 nm – 544 nm) for the anti-spot nanobody detection, 552 nm (emission 56 2 nm – 636 nm) for anti–myc/Rhodamine detection, 405 nm (emission 412 nm – 467 nm) for 4′,6–diamidino–2–phenylindole (DAPI) (nuclei detection) and 638 nm (emission 648 nm – 750 nm) for γ–tubulin/Alexa647. The excitation wavelength for chlorophyll was 488 nm (emission 764 nm – 769 nm). For fixed-cell imaging, a 40x oil–corrected objective was used (N.A. = 1.3; reflective index n20/D 1.516, pinhole adjusted to 1 airy unit) at RT.

2.6 | Quantifications and statistical analyses

Image analyses, root/leaf length and signal intensity were performed through Fiji v2.9.0/1.53 t (rsb.info.nih.gov/ij). Co-localization was analyzed using Pearson Correlation Coefficient statistics, through the Coloc2 tool in Fiji. Statistical analysis and generation of graphs were done on GraphPad Prism [version 10.1.1 (270)]. The significance threshold was set at *p*-value <0.05 and the exact values are shown in graphs. For tests involving multiple comparisons, one–way ANOVA was used followed by Dunnet's or Dunn's multiple comparison tests to define whether differences were statistically significant (or as indicated). Details of the statistical tests applied, including the choice of statistical method, the number of biological replicates (N) and the exact number of technical replicates (n) are indicated in the corresponding figure legend.

3 | RESULTS AND DISCUSSION

3.1 | Spot-tag method establishment for plant cells

KIN7.3, along with the caspase-like protease SEPARASE (also known as "extra spindle poles", ESP), forms part of the KISC (Moschou et al. 2016). KISC modulates cell polarity and microtubule (MT) dynamics during plant growth (Moschou et al. 2016, Liu et al. 2023b). Both KIN7.3 and ESP are recruited on the plasma membrane in root cells through a tether, the SEC–FOURTEEN HOMOLOGUE 8 (SFH8) (Liu et al. 2023b). KIN7.3 and ESP can also show a partial MT localization.

We examined the applicability of spot-tagging by generating stable *Arabidopsis thaliana* lines expressing KIN7.3 fused to His/FLAG epitopes, along with N-terminal spot-tag and C-terminal myc- or tagRFP sequences. We drove the expression of these constructs under the meristematic-specific promoter RPS5a (*RPS5apro:HF–spot–KIN7.3–myc* and *RPS5apro:HF–spot–KIN7.3–tagRFP*). However, the tagRFP in the *RPS5apro:HF–spot–KIN7.3–tagRFP* stable lines did not produce a sufficient signal, likely due to the low quantum yield of tagRFP and the overall low levels of KIN7.3 (see also below). Therefore, we refer to this line as "*RPS5apro:HF–spot–KIN7.3*" hereafter. The constructs *RPS5apro:HF–spot–KIN7.3–myc* or *RPS5apro:HF–spot–KIN7.3* could at least partially rescue the shorter root phenotype of the triple loss-of-function mutant of the KIN7.3 – clade, *kin7.1 kin7.3 kin7.5* (Moschou et al. 2016). Furthermore, we observed that these constructs could also rescue the elongated and curly leaf/cotyledon phenotype reported herein (*k135*; Figure S1A–C). Live imaging detection of anti-spot nanobody fluorescence was successful, albeit only in the outermost root cell layers (Figure S2A; i.e., epidermal cells).

As the spot signal was confined in the outermost cell layers (i.e., epidermis), we assumed that the anti-spot nanobody could not reach the innermost cell layers. This live-imaging approach, however, could still be valid for the rapid localization of proteins in epidermal cells. To test our assumption of low spot nanobody penetrance, we developed a whole-mount protocol for spot-tagging of Arabidopsis root tip fixed-cells (Figure 1A). We incubated fixed roots in fluorescent anti-spot nanobodies for 2 h at RT or overnight at 4°C and we counterstained anti-spot-labelled roots with anti-myc (Figure 1B). We titrated the nanobody (1:50–1:2,000) and used as negative control untransformed wild–type (WT) roots of the same ecotype (Figure S2B). We detected colocalized myc/spot signals only in transformed lines (*RPS5apro:HF–spot–KIN7.3–myc*), albeit with a rather low intensity (Figure 1B). This result is consistent with the reported low levels of KIN7.3 in root cells (Moschou et al. 2016). Furthermore, we tested whether the spot signal colocalized with MTs. While KIN7.3 can partially bind MTs, KISC–SFH8 localization on the plasma membrane of root cells is likely independent of MTs (Liu et al. 2023b). We could confirm this finding following treatments with the MT stabilizing drug taxol or upon the destabilizing drug oryzalin application on *RPS5apro:HF–spot–KIN7.3* expressing seedlings (Figure 1C). Noteworthy, we could detect higher levels of KIN7.3 on the plasma membrane, compared to the ones we observed in our previous studies (taxol treated root cells, lower panel; Figure 1C). This result could imply that the previously used GFP-tagged KIN7.3 may be subjected to stereochemical hindrance at the plasma membrane, which restricts its avidity for SFH8. This hindrance likely depends on the fact that KIN7.3 enters a tightly packed state on the membrane, together with SFH8 [i.e., a liquid–liquid phase condensate (Hatzianestis et al. 2023, Liu et al. 2023b)]. We further observed that HF–spot–Kin7.3 could also enter the nucleus and localized there more than the corresponding signal observed by the GFP–KIN7.3 line [GFP–KIN7.3/35Spro:tagRFP–$MAP4^{MBD}$ (MT–binding domain of MICROTUBULE ASSOCIATED PROTEIN 4) marker; Figure 1D]. Taken together, these data suggest that spot-tagging could efficiently localize KIN7.3 and could surpass the limitations of the potential stereochemical hindrance exerted by tight packing.

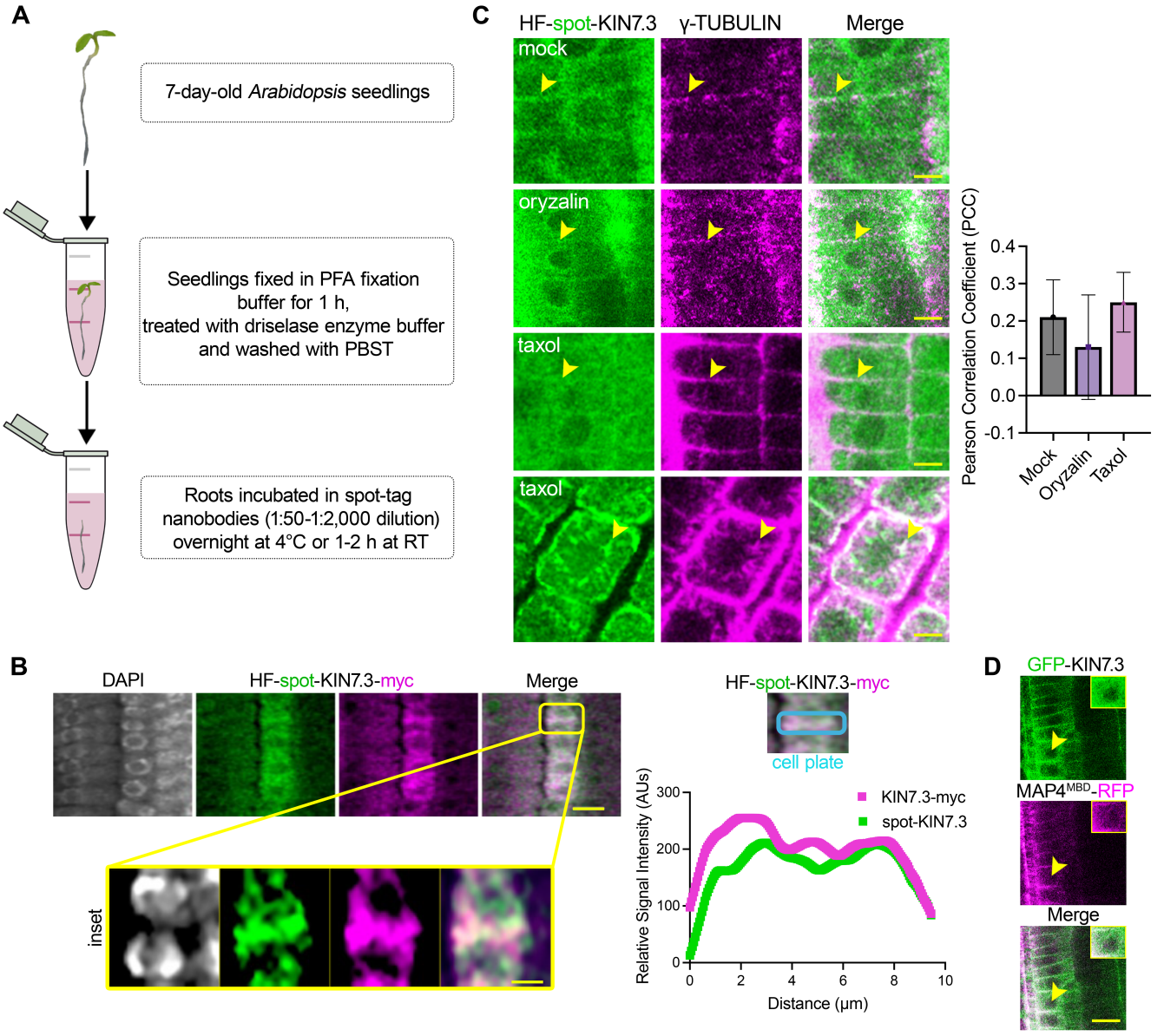

FIGURE 1 **Spot-tag experimental pipeline in stable Arabidopsis transgenic lines carrying spot–KIN7.3. (A)** Experimental pipeline for spot-tag detection in fixed root epidermal, meristematic cells. PFA, Paraformaldehyde; PBST, PBS/Tween20. **(B)** Left: Confocal micrographs showing the detection of the ATTO488 spot-nanobody and myc/Rhodamine signal in root epidermis meristematic cells. Roots are counterstained with DAPI for nuclei visualization. Scale bars, 10 μm. Right: Colocalization analysis as relative signal intensity of the spot nanobody and the –myc tag on the cell plate denoted by the blue box; The experiment was repeated more than ten times with similar results (N > 10 biological replicates, n = 3 technical replicates). HF; His-FLAG, AUs; Arbitrary Units.**(C)** Confocal micrographs showing the detection of the ATTO488 spot–nanobody recognizing spot–KIN7.3 (RPS5apro:HF–spot–KIN7.3) and γ–TUBULIN in root epidermal meristematic cells in mock conditions and upon taxol (10 μM at RT for 1 h) and oryzalin (10 μM at RT for 1 h) treatments, for MT destabilization and stabilization, respectively. Yellow arrows indicate KIN7.3 and γ– TUBULIN co-localization. We provide two different types of root cells in taxol-treated samples (differential MT stability) to denote the retention of KIN7.3 on the plasma membrane in the presence of taxol. Scale bars, 5 μm. Pixel colocalization analysis using Pearson Correlation Coefficient (PCC) was ~ + 0.2–0.3 and is indicated in the respective graph on the right; The experiment was repeated four times (N = 4 biological replicates, n = 3 technical replicates). HF; His-FLAG **(D)** Confocal micrograph of Arabidopsis lines co-expressing KIN7.3pro: GFP–KIN7.3 and the MAP4^{MBD} MT marker. Arrows and respective insets indicate the diffused nuclear signal of KIN7.3 in the stable line. The experiment was repeated four times (N = 4 biological replicates, n = 3 technical replicates). Scale bar, 10 μm.

3.2 | KIN7.3 detection by anti-spot nanobodies in *Nicotiana benthamiana*

Nicotiana benthamiana is widely used by the research community for the rapid interrogation of protein localization. We thus asked whether this system can be used for spot-tagging. We first attempted infiltration of the anti-spot nanobody in intact leaves of *N. benthamiana* leaves, which had also been infiltrated with a construct carrying *KIN7.3pro:spot–KIN7.3*. Under this experimental setting, we could not detect the spot signal. We thus conclude that the anti-spot nanobody cannot be taken up by intact leaf cells, at least in our settings.

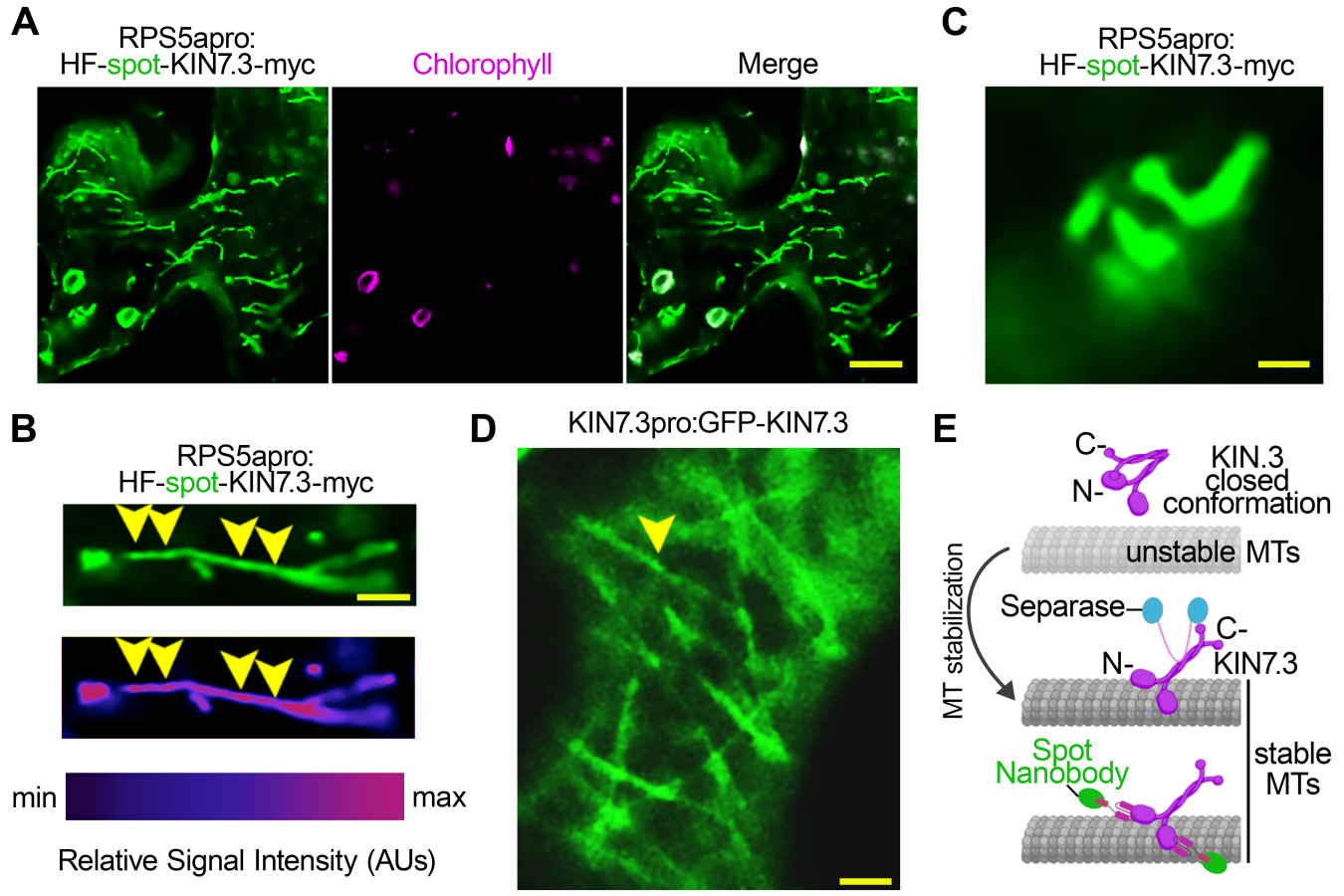

FIGURE 2 **Transient expression and detection of *spot–KIN7.3* or *GFP–KIN7.3* in *N. benthamiana* mesophyll cells. (A)** Confocal micrographs showing the detection of the ATTO488 spot-nanobody, recognizing spot–KIN7.3 (*RPS5apro*:HF–spot–KIN7.3–myc), transiently expressed in wounded areas of *N. benthamiana* leaf cells. Scale bar, 10 μm. The experiment was repeated three times (N = 3 biological replicates, n = 3 technical replicates). HF; His-FLAG **(B)** Upper: Confocal micrographs showing the detection of ATTO 488 spot-nanobody recognizing spot–KIN7.3 showing a "bead-like signal" (denoted with yellow arrowheads as uneven signal distribution on the filaments). Lower: spectrum visualization of the "bead-like" spot–KIN7.3 signal. The spectrum intensity scale is shown below the spectrum micrograph; note the uneven intensity of the signal. AUs, arbitrary units. Scale bar, 2 μm. The experiment was repeated three times (N = 4 biological replicates, n = 3 technical replicates). HF; His-FLAG **(C)** Confocal micrographs showing the arrangement of MTs, likely imposed by tension due to overstabilization effect and/or overaccumulation of spot–KIN7.3. Scale bar, 2 μm. The experiment was repeated three times (N = 3 biological replicates, n = 3 technical replicates). HF; His-FLAG **(D)** Confocal micrographs showing the detection of GFP–KIN7.3 expressed under its native promoter. The yellow arrow shows the filament-like localization of KIN7.3. Note the increased and diffused cytoplasmic signal. Scale bar, 5 μm. The experiment was repeated more than ten times (N > 10 biological replicates, n = 3 technical replicates). **(E)** Model of KIN7.3 activation and binding of MTs. In the absence of spot nanobodies, KIN7.3 is in the closed conformation (upper). ESP binds on the non–motor C–terminus tail domain, thereby blocking N/C–termini interaction of KIN7.3 (middle) and resulting in KIN7.3 binding on MTs and stabilizing them. Hence, spot nanobodies binding on the N-terminus of spot–KIN7.3 leads to a KIN7.3 "open conformation" that allows binding on MTs and their stabilization.

Hence, to overcome the physical barrier constructed by the cell wall in intact leaf cells that could restrict the nanobody uptake, we introduced small wounds to the leaves. To achieve this wounding, we used a razor blade and incubated the leaves with the anti-spot nanobody for 1 h at RT. Under this setting, we could detect high-intensity signals of KIN7.3 filaments in cells proximal to the wounds (Figure 2A). Our results suggest that this simple wounding approach is sufficient to allow the uptake of anti-spot nanobodies. We cannot discount the possibility that under conditions of cell expansion, where the porosity of the wall may increase, the cell could also take up anti-spot nanobodies. Furthermore, although we could see KIN7.3 filaments, their structure was aberrant and did not resemble the typical MTs that we could see with KIN7.3 expressed as GFP fusion.

3.3 | Spot-tagging reveals details of KIN7.3 localization transiently

Given the observed stability of the anti-spot nanobody signal, we carried out a thorough examination of the filamentous localization of KIN7.3 in *N. benthamiana*. Subcellular localization of KIN7.3 was not compromised by the spot-tagging as almost all the signal appeared filamentous (Figure 2A). Surprisingly, KIN7.3-spot signal, depicted also by intensity spectrum visualization, decorated unevenly these filaments (Figure 2B). On the contrary, the *KIN7.3pro:GFP–KIN7.3* construct under the same conditions (Figure 2C, D), produced increased fluorescence in the cytoplasm. This result, like in the case of KIN7.3 binding on the plasma membrane mentioned above, suggests that GFP leads to stereochemical

hindrance, which may restrict the localization of KIN7.3 on these filaments. Moreover, some KIN7.3 filaments were likely under tension, perhaps because spot-tagging allows the stabilization of KIN7.3 probably on MTs (Figure 2C). We have previously shown that efficient MT-binding by KIN7.3 depends on the "open conformation" of KIN7.3 where N- and C-termini of KIN7.3 are far apart due to the C-terminal binding of ESP (Moschou et al. 2016). The anti-spot nanobodies may thus block the intramolecular interaction between N- and C-termini of KIN7.3, thereby promoting MT-binding (or other filamentous localization) and stabilization (a model is presented in Figure 2E). Hence, we can speculate for now that exogenous application of the anti-spot nanobodies can enhance the stability of MTs by letting KIN7.3 bind on them.

We foresee that our spot-tagging pipeline can be widely applicable in plant cell biology. We also confirm the high quantum yield of ATTO probes and their photostability, which may allow for gaining finer images. This ability of spot-tagging may make it a good fit for proteins with low levels of expression (e.g., by improving the photostability and quantum yields). Hence, spot-tagging may enable single-molecule localization microscopy (SMLM) techniques, providing outstanding spatial resolutions surpassing limitations, such as poor photon emission or detection efficiency, low fluorophore labelling densities, linkage errors or steric hindrances. The protocol is much more rapid (1–2 h staining) than common immuno-labelling procedures. Furthermore, spot-tagging can help in delineating localization in detail and can reduce the stereochemical hindrance imposed by large FPs. It is also worth considering spot nanobodies as activators of KIN7.3 with potential implications in functional studies in living cells, at least in root epidermal cells that were permeable to the anti-spot nanobody. However, there are some inherent limitations of the spot-tagging approach. Spot nanobodies cannot enter intact leaf plant cells unless cells are mechanically damaged (e.g., wounded) and this may affect the physiology and thus localizations. Additionally, spot nanobody detection sometimes creates a noisy background during imaging and can confound 3D image rendering. Finally, for now, there are only two nanobodies available (nanobodies carrying ATTO488 and ATTO594), limiting fluorescence combinations in imaging.

AUTHOR CONTRIBUTIONS

Conceptualization: PNM, CL, AM; Methodology: CL, AM; Investigation: CL, AM; Visualization: AM; Funding acquisition: PNM; Project administration: PNM; Supervision: PNM; Writing – original draft: PNM, AM; Writing – review & editing: AM, PNM, CL.

ACKNOWLEDGEMENTS

We thank the members of the Moschou Lab for the fruitful discussions.

FUNDING INFORMATION

This work was supported by the EU Marie Skłodowska Curie–RISE Action ('PANTHEON' 872969; PNM), IMBB–FORTH start–up funding (PNM), Hellenic Foundation of Research and Innovation–Always Strive for Excellence–Theodoros Papazoglou ('NESTOR', 1264; PNM), Fondation Sante (PNM) and the Hellenic Foundation of Research and Innovation PhD scholarships (06526; AM).

DATA AVAILABILITY STATEMENT

The data and materials that support the findings of this study are available from the corresponding author upon reasonable request.

ORCID

Andriani Mentzelopoulou https://orcid.org/0000-0003-4266-8714
Chen Liu https://orcid.org/0000-0002-1604-0694
Panagiotis Nikolaou Moschou https://orcid.org/0000-0001-7212-0595

REFERENCES

Clough SJ, Bent AF (1998) Floral dip: a simplified method for Agrobacterium–mediated transformation of Arabidopsis thaliana. *Plant J* 16(6): 735–743

Hatzianestis IH, Mountourakis F, Stavridou S, Moschou PN (2023) Plant condensates: no longer membrane–less? *Trends Plant Sci*

Johansen, L. K., & Carrington, J. C. (2001). Silencing on the Spot. Induction and Suppression of RNA Silencing in the Agrobacterium-Mediated Transient Expression System. *Plant Physiology*, 126(3), 930–938. https://doi.org/10.1104/PP.126.3.930

Liu C, Mentzelopoulou A, Muhammad A, Volkov A, Weijers D, Gutierrez–Beltran E, Moschou PN (2023a) An actin remodeling role for Arabidopsis processing bodies revealed by their proximity interactome. *Embo J* 42(9): e111885

Liu C, Mentzelopoulou A, Papagavriil F, Ramachandran P, Perraki A, Claus L, Barg S, Dormann P, Jaillais Y, Johnen P, Russinova E, Gizeli E, Schaaf G, Moschou PN (2023b) SEC14–like condensate phase transitions at plasma membranes regulate root growth in Arabidopsis. *PLoS Biol* 21(9): e3002305

Liu C, Mentzelopoulou A, Hatzianestis IH, Tzagkarakis E, Skaltsogiannis V, Ma X, Michalopoulou VA, Romero–Campero FJ, Romero–Losada AB, Sarris PF, Marhavy P, Bolter B, Kanterakis A, Gutierrez–Beltran E, Moschou PN (2024) A proxitome–RNA–capture approach reveals that processing bodies repress coregulated hub genes. *Plant Cell* 36(3): 559–584

Moschou PN, Gutierrez–Beltran E, Bozhkov PV, Smertenko A (2016) Separase Promotes Microtubule Polymerization by Activating CENP–E–Related Kinesin Kin7. *Dev Cell* 37(4): 350–361

Nakagawa T, Kurose T, Hino T, Tanaka K, Kawamukai M, Niwa Y, Toyooka K, Matsuoka K, Jinbo T, Kimura T (2007) Development of series of gateway binary vectors, pGWBs, for realizing efficient construction of fusion genes for plant transformation. *Journal of Bioscience and Bioengineering* 104(1): 34–41

Schnitzbauer J, Strauss MT, Schlichthaerle T, Schueder F, Jungmann R (2017) Super–resolution microscopy with DNA–PAINT. *Nat Protoc* 12(6): 1198–1228

Virant D, Traenkle B, Maier J, Kaiser PD, Bodenhöfer M, Schmees C, Vojnovic I, Pisak–Lukáts B, Endesfelder U, Rothbauer U (2018) A peptide tag–specific nanobody enables high–quality labeling for dSTORM imaging. *Nat Commun* 9(1): 930

SUPPORTING INFORMATION

Additional supporting information can be found online in the Supporting Information section at the end of this article.

How to cite this article: Mentzelopoulou, A., Liu, C. & Moschou, P.N. (2024) Protein Detection and Localization in Plant Cells Using Spot-Tagging. *Physiologia Plantarum*, 176(3), e14351. Available from: https://doi.org/10.1111/ppl.14351